

Prediction Accuracy of Color Imagery from Hyperspectral Imagery

Peter Bajcsy and Rob Kooper

National Center for Supercomputing Applications (NCSA)
University of Illinois at Urbana-Champaign, IL
Email: pbajcsy@ncsa.uiuc.edu, kooper@ncsa.uiuc.edu

ABSTRACT

In this paper we present the utilization of high-spectral resolution imagery for improving low-spectral resolution imagery. In our analysis, we assume that an acquisition of high spectral resolution images provides more accurate spectral predictions of low spectral resolution images than a direct acquisition of low spectral resolution images. We illustrate the advantages by focusing on a specific case of images acquired by a hyperspectral (HS) camera and a color (red, green, and blue or RGB) camera. First, we identify two directions for utilization of HS images, such as (a) evaluation and calibration of RGB colors acquired from commercial color cameras, and (b) color quality improvement by achieving sub-spectral resolution. Second, we elaborate on challenges of RGB color calibration using HS information due to non-ideal illumination sources and non-ideal hyperspectral camera characteristics. We describe several adjustment (calibration) approaches to compensate for wavelength and spatial dependencies of real acquisition systems. Finally, we evaluate two color cameras by establishing ground truth RGB values from hyperspectral imagery and by defining pixel-based, correlation-based and histogram-based error metrics. Our experiments are conducted with three illumination sources (fluorescent light, Oriel Xenon lamp and incandescent light); with one HS Opto-Knowledge Systems camera and two color (RGB) cameras, such as Sony and Canon. We show a data-driven color-calibration as a method for improving image color quality. The applications of the developed techniques for HS to RGB image calibrations and sub-spectral resolution predictions are related to real-time model-based scene classification and scene simulation.

KEYWORDS: Spectral data exploitation, calibration, hyperspectral and RGB imagery

1 INTRODUCTION

Perhaps, it is appropriate to start by introducing the terms color and hyperspectral imagery. Both types of imagery are defined over the visible spectrum range that covers wavelengths from 400 nm to 700 nm. Color imagery is usually understood as a three value representation (red, green and blue; or RGB) of the visible spectrum, where each value represents a sub-range of wavelengths, e.g., blue is [400nm, 500nm], green is [500nm, 600nm] and red is [600nm, 700nm]. Most of the commercial cameras deliver color imagery according to some representation of the three basic colors. Hyperspectral imagery is represented by more than three values corresponding to narrow sub-ranges of visible or near-infrared wavelengths. Although hyperspectral cameras are much more expensive than color cameras, they provide higher spectral discrimination of colors. For example, while red color can be discriminated by the magnitude of the red value in color imagery, it can be discerned much more precisely by comparing the magnitudes of multiple values in hyperspectral imagery.

The high spectral resolution of hyperspectral (HS) imagery has been taken advantage in several applications where accurate discrimination is the main objective. For instance, there are numerous reports on the use of hyperspectral imagery for discriminating minerals, crops, or land use and land covers^{18,19,20,21}. In these applications, the main emphasis is on the accuracy of material classification based on its surface appearance measured by spectral reflectivity at multiple

wavelengths. The processing is performed off-line and might require the use of supercomputers²³. However, there exists another class of applications where real-time processing and camera cost are critical for successful system deployment. For example, modeling scene clutters for target detection from aerial photography should be performed in real-time with relatively inexpensive, light-weight and rugged color cameras that can be mounted on surveillance drones or unmanned aerial vehicles (UAVs). Our work aims at supporting designs of real-time and inexpensive systems for accurate color scene prediction that would be used for target detection.

One should also be aware that the use of hyperspectral imagery requires significant storage and computational resources. Furthermore, due to the amount of data being acquired and transferred, it is hard to perform acquisition and processing in real-time. Thus, it would be beneficial for real-time applications to use inexpensive and fast color cameras, and perform model-based classification or simulation of color imagery using hyperspectral information that was acquired off-line and pre-processed. The utilization of HS information for improving color scene prediction and understanding the color camera processing pipeline¹⁵ is the main motivation of our work.

In order to realize a system for model-based scene analysis with real-time color imagery and predicted color imagery from hyperspectral information, one has to develop three major components. First, there has to be an efficient representation of hyperspectral imagery acquired off-line. This component strives to preserve maximum spectral information while (a) reducing HS data size and (b) speeding up HS information retrieval. The challenge of this component also lies in building a large enough database for multiple scene clutter types that vary due to varying elevation, illumination and viewing angles⁹, as well as due to changing object surface properties (e.g., seasonal changes). This problem of building bi-directional reflectance and texture databases from RGB images^{10,11,12} has been addressed in the past.

Second, one has to develop hyperspectral to color imagery mappings. These mappings have to incorporate variables, such as specific CCD sensors, camera optics, propagation media, illumination sources, and the distances between cameras and object surfaces. We assume that spatial mappings for any predicted scene are available from multiple GIS products, e.g., elevation maps, land use and land cover maps, and the problem is primarily defined as prediction of RGB values. Finally, there is a need to improve the quality of color imagery using hyperspectral information. Although it is expected that a color scene prediction would be more accurate using HS information than using RGB information, the approaches have not been outlined and the benefits have not been quantified in the past.

In this work, our focus is on the second component, such as developing hyperspectral to color imagery mappings. For the first component, we leverage our previous work on efficient modeling of bidirectional texture functions (BTFs) from HS imagery^{8,13}. We could use multiple statistical models for representing HS images (Gaussian, Weibull and Johnson family distributions³) that represent an efficient BTF model. For the third component, we re-use several metrics developed for evaluating statistically predicted and measured imagery⁸. In the past, several standard HS to RGB mappings have been proposed, for example, the Bruton's method¹⁶ and its implementation in the I2K software¹⁴. These mappings could be used for visualization purposes since viewing high dimensional HS image is still an open problem. The RGB representation of HS imagery provides the most familiar display of visible spectrum information for humans. However, these mappings assume that cameras acquire values independent of sensors, illumination, and propagation media. These assumptions are violated when working with real cameras and acquiring images of outdoor scenes. Thus, our goal is to evaluate HS to RGB color mappings in order to quantitatively improve the quality of color (RGB) images using HS information.

In the rest of this paper, we elaborate on the use of a hyperspectral (HS) camera and a color (red, green, and blue or RGB) camera. First, we identify two directions for utilization of HS images, such as (a) for evaluation and calibration of RGB colors acquired from commercial color cameras, and (b) for sub-spectral resolution improvement of image quality. Second, we elaborate on challenges of RGB color calibration using HS information due to non-ideal illumination sources and non-ideal hyperspectral camera characteristics. We describe several adjustment approaches to compensate for wavelength and spatial dependencies of real acquisition systems. Finally, we evaluate two color cameras by establishing ground truth RGB values from hyperspectral imagery and by defining pixel-based, correlation-based and histogram-based error metrics. Our experiments are conducted with three illumination sources (fluorescent light, Oriol Xenon lamp and incandescent light); with one HS OptoKnowledge camera and two color (RGB) cameras, such as Sony and Canon. We show a data-driven color-calibration as a method for improving image color quality. The applications of such HS to

RGB image calibrations and sub-spectral resolution predictions are related to real-time model-based scene classification and scene simulation. The developed techniques for HS to RGB mapping and their accuracy evaluations enable to better exploit spectral data, calibrate low end cameras for airborne data collections, incorporate data quality control for collections of spectral data and relate multiple spectral libraries of bidirectional reflectance distribution functions (BRDFs). We believe that the main contributions of this paper lie (1) in describing the utilization of HS images for improving RGB color quality of color images, and (2) in providing a summary of evaluation and calibration issues related to any calibration efforts of low-spectral resolution imagery with high-spectral resolution imagery.

2 PROBLEM OVERVIEW

We assume that an acquisition of high spectral resolution images provides more accurate spectral predictions of low spectral resolution images than a direct acquisition of low spectral resolution images. Based on this assumption, one can utilize high spectral resolution imagery either for evaluating and calibrating colors of low spectral resolution cameras, or for increasing spectral resolution of low resolution cameras using additional information about scenes. To illustrate these two approaches to the utilization of high spectral resolution imagery, we have focused on the case of hyperspectral (larger than three-dimensional spectral information) and color (three-dimensional spectral information) imagery. The two approaches are shown in Figure 1.

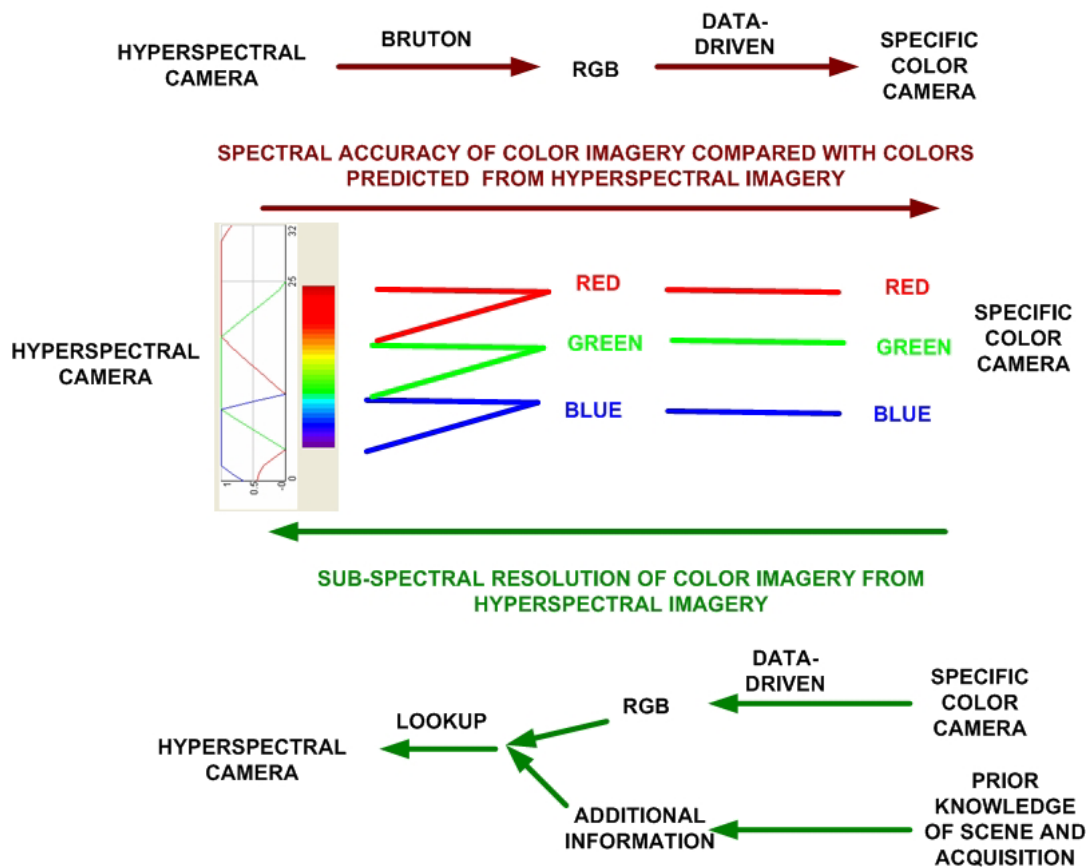


Figure 1: Two approaches how to utilize high spectral resolution imagery for improving color (RGB) imagery.

For the problem described in this paper, we should add another assumption about dynamic range of spectral values. We assume that the dynamic range of any hyperspectral measurement at any image location is larger than the dynamic range of a color (RGB) measurement at the same spatial location. Thus, it is always possible to obtain a low-dimensional (3D

in our case) spectral value from high-dimensional measurements. For instance, this assumption would not hold if 2D spectral measurements with 2 bits per pixel accuracy would have to predict 1D spectral measurement with 16 bits per pixel accuracy.

3 SPECTRAL ACCURACY OF COLOR IMAGERY COMPARED WITH RGB COLORS PREDICTED FROM HYPERSPECTRAL IMAGERY

The first task of evaluating and calibrating RGB colors of color cameras using a hyperspectral camera can be approached under various assumptions about hyperspectral cameras and illumination sources. We present the issues related to establishing ground truth RGB values from hyperspectral images in Section 3.1 before we outline the RGB color evaluation and calibration of commercial color cameras using the hyperspectral information in Section 3.2.

3.1 Establishing Ground Truth RGB Values from Hyperspectral Images

We summarized ideal and non-ideal characteristics of hyperspectral cameras and illumination sources in Table 1. The word ideal camera refers to equal sensitivity of the camera to different wavelengths of incoming visible spectrum light without any spatial and temporal variation of measured intensities due to mechanical, optical or electronic camera limitations (e.g., spherical aberration, optical or mechanical vignetting, and spurious electronic currents). The word ideal illumination source refers to a flat irradiance spectrum over visible spectrum wavelengths, and temporally invariant and spatially uniform (diffused) illumination. In the rest of this section, we will assume temporal invariance of camera and illumination.

Table 1: A summary of ideal and non-ideal characteristics of hyperspectral cameras and illumination sources. The summary assumes temporal invariance of camera and illumination.

HS Camera\Illumination	Ideal	λ -dependency	(x,y) dependency	λ -dependency and (x,y) dependency
Ideal	Case 1: HS->Ground Truth RGB	Case 2a: Exposure =f(λ)	Case 2b: Illumination calibration	Case 2a+2b: Exposure =f(λ) and Illumination calibration
λ -dependency	Case 3a: Exposure =f(λ)			
(x,y) dependency	Case 3b: Optics calibration			
λ -dependency and (x,y) dependency	Case 3a+3b: Exposure =f(λ) and Optics calibration	Case 4a	Case 4b	Case 4c

Case 1 - Ideal hyperspectral camera and ideal illumination source: First, let us assume that we have an ideal hyperspectral camera and an ideal illumination source. Under these assumptions about ideal light and a hyperspectral camera, one can convert hyperspectral values into color (RGB) values using the Bruton’s transformation method¹⁶ as implemented in the I2K software¹⁴. These RGB values converted from hyperspectral values can be directly used as ground truth values for evaluating and calibrating commercial color cameras.

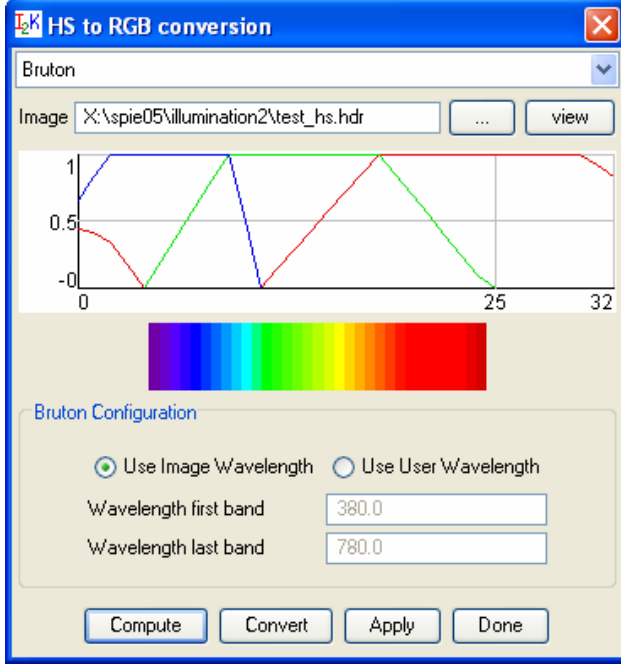


Figure 2: Hyperspectral to RGB transformation according to Bruton¹⁶ as developed in the I2K software¹⁴.

Case 2 - Ideal hyperspectral camera: Second, let us assume that a hyperspectral camera is ideal but an illumination source is not ideal. In this case, one has to compensate camera intensities for their spatial and wavelength dependencies. The spatial compensation (Case 2b in Table 1), also denoted as illumination calibration, is achieved by applying the following formula:

$$\rho(x, y, \lambda) = \frac{[I_{measured}(x, y, \lambda) - I_{black}(x, y, \lambda)]}{[I_{white}(x, y, \lambda) - I_{black}(x, y, \lambda)]} \quad (1)$$

where $\rho(x, y, \lambda)$ is the illumination-calibrated image also referred to as a reflectance image, I_{black} is the image acquired with lens cap on that measures camera noise (dark camera current), and I_{white} is the image obtained by placing a calibration board in front of the camera with reflectivity close to 100% (in our case about 97-99%). The illumination calibration assumes that propagation media and camera-object distances are constant. The black and white images are also denoted as black body and white body images for a specific light source.

The wavelength dependency (Case 2a in Table 1) can be modeled by estimating the dynamic range per each wavelength for a highly reflective scene, such as the white calibration board. The exposure time for acquiring images at each wavelength is then adjusted to be inversely proportional to the dynamic range of the acquired image for the white calibration board according to the equation below.

$$\text{Coef}_{\text{exposure time}}(\lambda_i) = \frac{\text{Max}[|I_{\text{max}}(\lambda_i) - I_{\text{min}}(\lambda_i)|; \forall i = 1, 2, \dots, \text{numWavelength}]}{|I_{\text{max}}(\lambda_i) - I_{\text{min}}(\lambda_i)|} \quad (2)$$

where $\text{Coef}_{\text{exposure time}}$ is the multiple of the current exposure time to achieve equal dynamic range for all wavelength images, I_{min} and I_{max} are the minimum and maximum values per wavelength image (band image) and the nominator is the global maximum over all wavelength images. If both wavelength and spatial dependencies are present (Case 2a+2b in Table 1) then both illumination calibration and exposure time adjustment should be performed.

In our experiments, we have simulated these three scenarios by using fluorescent light (laboratory ceiling light), Xenon light (Oriel Xenon lamp¹⁷, 160W) and incandescent light (regular desktop lamp, 60W). The Oriel Xenon lamp can be

viewed as wavelength independent according to the Oriel manufacturer’s specification. The fluorescent ceiling light can represent a spatially uniform illumination source. Finally, the incandescent light is a point light source that demonstrates wavelength and spatial dependencies.

Case 3 - Ideal illumination source: Third, let us assume that a hyperspectral camera is not ideal but an illumination source is ideal. In this case, one has to compensate for wavelength and spatial dependencies. The wavelength dependency (Case 3a in Table 1) that represents an unequal sensitivity of the hyperspectral camera to different wavelengths of incoming visible spectrum light was measured in the experimental camera manufactured by OptoKnowledge Inc.⁵ under the Oriel Xenon lamp illumination (wavelength independent in the visible spectrum). Figure 3 illustrates a particular wavelength dependency from blue to red wavelengths. This dependency can be compensated by adjusting wavelength dependent exposure times according to the equation (2).

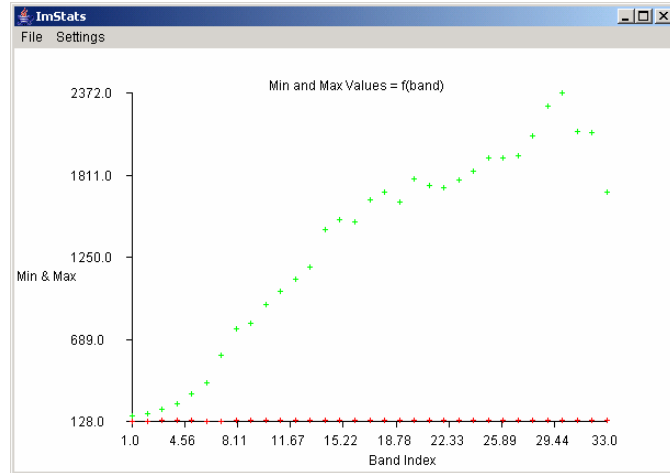


Figure 3: Wavelength dependent dynamic range (Min and Max raw values) measured by acquiring hyperspectral image of a white calibration board with reflectance approximately 97% at EL=45 and AZ=0. The band index one corresponds to 440nm and band index 29 to 720nm

The spatial dependency (Case 3b in Table 1) represents variations of measured intensities due to mechanical or optical camera limitations (e.g., spherical aberration or vignetting). To adjust for spatial dependency, one could use theoretical models for known parameters of optics components or apply the illumination calibration according to equation (1). If both wavelength and spatial dependencies are present (Case 3a+3b in Table 1) then both optics calibration and exposure time adjustment should be performed.

Case 4 - Non-ideal hyperspectral camera and non-ideal illumination source: Fourth, let us assume that a hyperspectral camera is not ideal and an illumination source is not ideal. One would apply all calibration adjustments to compensate for spatial and wavelength dependencies. The question arises whether RGB values predicted from adjusted hyperspectral images can still be viewed as ground truth RGB values for evaluating and calibrating RGB colors obtained from commercial color cameras. Furthermore, if the adjustments are inaccurate then the assumptions of Bruton’s HS to RGB transformation would not hold and the transformation might introduce additional inaccuracy as well.

In our experiments, we have obtained measured hyperspectral images using fluorescent light (Case 4a), Oriel Xenon lamp (Case 4b), and incandescent light (Case 4c). We compare predicted RGB values from hyperspectral images for these three cases in order to illustrate the variations due to multiple adjustments.

3.2 Evaluation and Calibration of Color Cameras Using Predicted RGB Values

Evaluation and calibration of color (RGB) cameras can be executed by acquiring a hyperspectral image and multiple color images of the same scene containing the whole gamut of colors (e.g., color calibration disks or color calibration charts), and illuminated by an available light source that approximates characteristics of the ideal light. Hyperspectral and RGB images have to be illumination-calibrated to compensate for non-ideal illumination and spatially registered to

take into account misalignment due to different viewing angles. The illumination calibration is achieved according to Equation (1). The spatial registration is achieved by manually selecting matching points and computing affine transformation parameters to transform images to the reference coordinate system. Figure 4 shows the registration software I2K¹⁴ used for selecting matching points and verifying registration results. In our work, the reference coordinate system was set to the coordinate system of the reference hyperspectral image. We chose the affine transformation model since the camera view angle differences were small enough to be compensated by translation, rotation, scale and shear.

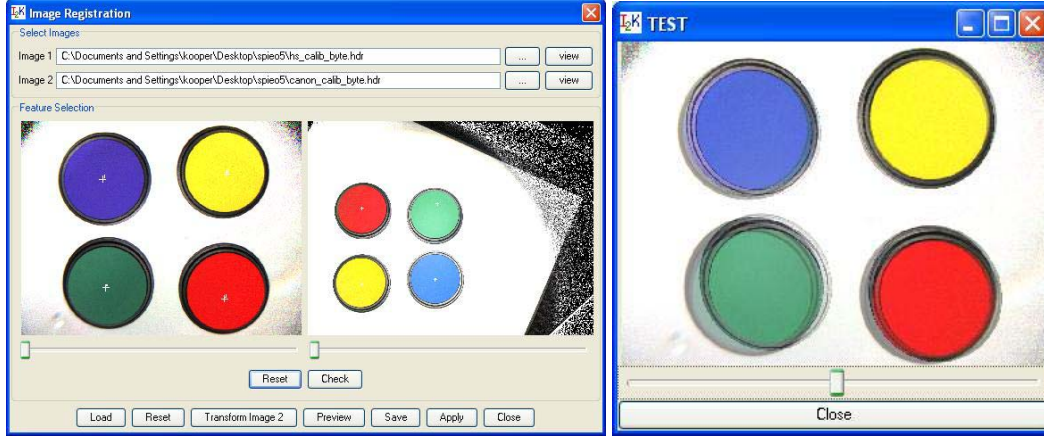


Figure 4: Registration of hyperspectral (left) and color images (middle) using affine transformation and manual point selection. Verification of registration alignment (right).

After illumination calibration and registration of measured scenes, the problem of evaluating color cameras can be solved by defining error metrics and applying them to (a) the directly measured RGB images and (b) the reference RGB images derived from hyperspectral images using the Bruton's transformation method¹⁶. In our experiments, we used the following three cameras. A hyperspectral camera manufactured by Opto-Knowledge Systems Inc.⁵ that is based on liquid crystal tunable filters^{6,7}. The hyperspectral camera generates 2D images with a large number of spectral bands corresponding to a set of selected wavelength ranges. Two color cameras that acquire RGB images are referred to as (a) the Sony camera (Sony SNC-RZ30N PTZ Pan/Tilt/Zoom Network Color Camera SNCRZ30N⁴), and (b) the Canon camera (Canon Power Shot SD100 Digital Elph).

Our quantitative comparisons use three error metrics including correlation-, pixel- and histogram-based comparisons as defined in our previous work⁸. The error metrics are defined below.

Correlation-Based Comparison: The correlation-based metric corresponds to a linear correlation coefficient r that is defined in Equation below.

$$r = \frac{\sum_i (x_i - x_{avg})(y_i - y_{avg})}{\sqrt{\sum_i (x_i - x_{avg})^2} \sqrt{\sum_i (y_i - y_{avg})^2}} \quad (3)$$

In this equation x_i are RGB values from HS images and y_i are RGB values from color images. The metric r is evaluated for red, green and blue bands separately. The correlation coefficient error metric r is also known as the Pearson correlation.

Histogram-Based Comparison: A histogram-based error metric $E_{ColorMis}^{Total}$ is the number of mismatched pixels in terms of their color between RGB values from HS images and RGB values from color images. The mathematical error definition is provided in Equation below. The metric $E_{ColorMis}^{Total}$ does not reflect how far apart the colors are. Instead, it captures the fact that a pixel was assigned a different color.

$$E_{ColorMis}^{Total}(band) = \frac{1}{2} \frac{1}{N_{HS \rightarrow RGB}} \sum_{i=1}^{numBins} \left\| h_{HS \rightarrow RGB}(band, i) - h_{RGB}(band, i) \frac{N_{HS \rightarrow RGB}}{N_{RGB}} \right\| \quad (4)$$

where h is the histogram value (frequency occurrence) of an intensity range falling into an i -th bin for one of the red, green or blue bands, N is the total number of image pixels, and the subscript $HS \rightarrow RGB$ refers to the predicted RGB values from hyperspectral values and RGB to the directly measured RGB values.

Pixel-Based Comparison: This metric refers to a direct pixel-to-pixel comparison. It is defined in Equations (5) and (6).

$$E_{Pixel}^{Total Avg} = \frac{1}{numBands} \sum_{band=1}^{numBands} E_{Pixel}^{Avg}(band) \quad (5)$$

where $numBands$ is the total number of bands in the evaluated image and

$$E_{Pixel}^{Avg}(band) = \frac{1}{numPixels} \sum_{i=1}^{numPixels} \|I_{HS \rightarrow RGB}(band, i) - I_{RGB}(band, i)\| \quad (6)$$

For RGB images, the band index takes the values of red, green and blue, and the $numBands$ is equal to three.

4 SUB-SPECTRAL RESOLUTION OF COLOR IMAGERY FROM HYPERSPECTRAL IMAGERY

The second task of developing a sub-spectral resolution imagery from color imagery is approached by building a database of bi-directional texture functions (BTF)^{1,2} for each clutter from high spectral resolution images¹³ that can be mapped to lower spectral resolution values as obtained from commercially available color (RGB) cameras. This approach is analogous to the sub-pixel (sub-spatial resolution) approach applied to target modeling in which the target geometry is used as the additional information to improve spatial resolution of acquired imagery. In our case of sub-spectral resolution scene modeling, the additional information comes from knowing scene clutter layout derived from, for instance, elevation, land use and land cover maps.

The objective of creating sub-spectral resolution images is to improve discrimination of objects and scene clutters. For example, if a reconnaissance flight should be conducted with its constraints on sensing equipment weight and cost then a real-time inexpensive color camera would provide sufficient information about a scene of interest. The acquired color imagery can be improved to increase its spectral resolution by incorporating scene layout knowledge. During the next day, a flight with hyperspectral camera can be conducted to acquire images with high spectral resolution. The high spectral resolution images can be compared to the expected hyperspectral imagery from the previous flight. The advantage of the comparison is the discrimination of camouflaged objects that have entered the scene of interest and would not have been discriminated from color (RGB) imagery. In this work, we do not report quantitative results about the benefits of hyperspectral imagery for the purpose of improving sub-spectral image resolution.

5 EXPERIMENTAL RESULTS

In order to demonstrate the benefits of high spectral resolution imagery for evaluating and calibrating colors of low spectral resolution cameras, we setup our hyperspectral camera, manufactured by Opto-Knowledge Systems Inc.⁵, to acquire image bands between 400nm and 700nm. We set the spectral spacing of 10nm between two adjacent bands and the exposure time of 30ms. Thus, we obtain a 30-dimensional vector of hyperspectral information that we map to a 3-dimensional vector of RGB information. Figure 5 illustrates several bands of a hyperspectral image that map to red, green and blue bands of the converted color image.

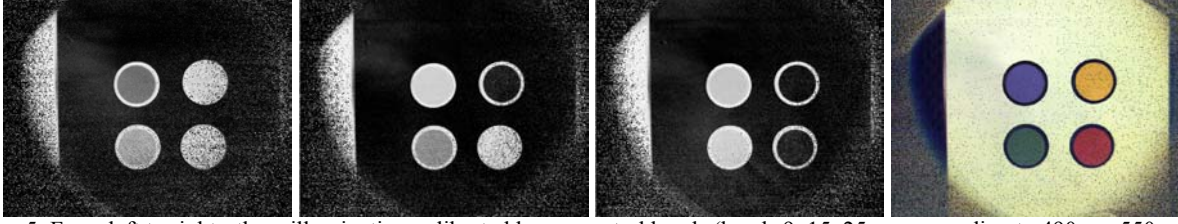


Figure 5: From left to right - three illumination-calibrated hyperspectral bands (bands 9, 15, 25 corresponding to 490nm, 550nm and 650nm) and the RGB image obtained by mapping hyperspectral bands to RGB using Bruton’s method. The hyperspectral images were acquired under Oriol Xenon lamp illumination. While the Oriol lamp provided a wavelength independent irradiance for the visible spectrum wavelength, one can observe spatial dependency of the illumination source.

5.1 Predictions of RGB Values from Hyperspectral Images under New Illumination Source

It is often the case that color (RGB) cameras are not illumination-calibrated and one would like to re-illuminate ground truth RGB values derived from calibrated HS measurements. In order to evaluate and calibrate RGB values of a scene obtained from uncalibrated color images, one would have to convert the hyperspectral image of a black body and a white body under the desired illumination to RGB, in addition to converting the calibrated hyperspectral image of the scene to RGB denoted as $\rho(x,y, \lambda)$, where λ is red, green or blue. Then, the ground truth RGB values $\rho(x,y, \lambda)$ would be re-illuminated according to the equation below.

$$I_{\text{re-illuminated}}(x, y, \lambda) = \rho(x, y, \lambda)[I_{\text{white}}(x, y, \lambda) - I_{\text{black}}(x, y, \lambda)] + I_{\text{black}}(x, y, \lambda) \quad (7)$$

where $I(x,y, \lambda)$ denotes the image value at row and column locations (x,y) , and the subscripts black and white correspond to the black body and white body images.

Figure 6 shows the results of our re-illumination experiments. First, we performed illumination-calibration of a HS image of a scene that was illuminated by Oriol Xenon lamp. The calibrated HS image was then converted to RGB image using Bruton’s transformation. Second, white hyperspectral images and black hyperspectral images were acquired under incandescent, fluorescent and Oriol Xenon lamp illumination. The white and black HS images were converted to RGB using Bruton’s transformation and applied to the calibrated RGB image of a scene. The resulting RGB images correspond to RGB images acquired by a color-calibrated camera under the chosen illumination.

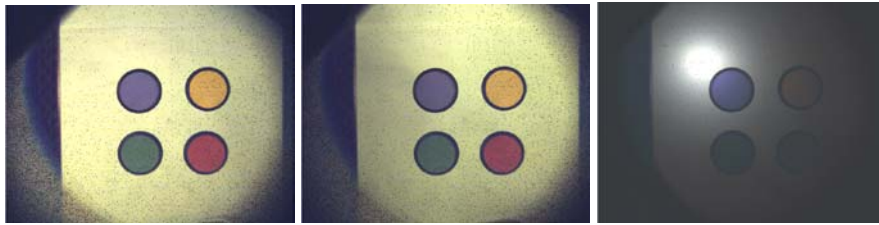


Figure 6: The results of re-illuminating RGB images formed from hyperspectral data and predicting the image appearances of color-calibrated cameras under three different illumination sources. Predicted RGB images from calibrated measured hyperspectral images under incandescent (left), fluorescent (middle) and Xenon (right) illumination. The HS images contained 30 bands, 10nm apart, wavelength range [400nm, 700nm]. All HS images were converted to RGB using the Bruton’s HS to RGB mapping.

5.2 Evaluation and Calibration of Color Cameras

In this experiment, we assume that our hyperspectral camera is non-ideal and the illumination source (Oriol Xenon lamp) has only spatial dependency. Thus, we establish our ground truth RGB values by performing wavelength-calibration of

HS camera, illumination-calibration of HS images and by applying Bruton’s hyperspectral to RGB transformation. The RGB images acquired from the two color cameras, such as Sony and Canon, have to be illumination-calibrated too since the illumination is characterized by spatial dependencies. After registering the three RGB images (two from color cameras and one from HS camera), we computed pair-wise error according to the metrics presented in Section 3.2. The pair-wise error is calculated between the RGB image predicted from HS image and the RGB image obtained by either Sony or Canon cameras. The three evaluated RGB images are shown in Figure 7.



Figure 7: Predicted RGB image from calibrated hyperspectral images (left), calibrated RGB image from Sony camera (middle) and calibrated RGB image from Canon color camera (right).

The error evaluations are summarized in Table 2. According to the table, the Sony and Canon cameras generate colors that are approximately equally similar (or dissimilar) to the ground truth RGB values derived from the hyperspectral images. According to the correlation-based and pixel-based error metrics, the Sony camera is slightly closer to the ground truth RGB values while according to the histogram-based error metric, either the Sony camera or the Canon camera would be closer depending on the band.

Table 2: RGB color evaluations of Sony and Canon color cameras.

Color Camera\Metric	Correlation-based	Histogram-based	Pixel-based
Sony	(0.817, 0.751, 0.862)	(0.748, 0.564, 0.668)	(32.49, 47.55, 40.51)
Canon	(0.760, 0.734, 0.836)	(0.752, 0.531, 0.563)	(41.20, 52.78, 44.85)

We can now perform color calibration of the two color cameras (Sony and Canon) by developing a data-driven mapping between the directly measured RGB values and the RGB values derived from HS images. In general, this mapping improves the colors with respect to the ground truth RGB values defined by the hyperspectral camera. The mapping consists of a 3x3 matrix of coefficients that are computed by solving an over-determined set of linear equations and using randomly selected image points. Figure 8 shows the random point selection and the resulting mappings for Sony and Canon cameras.

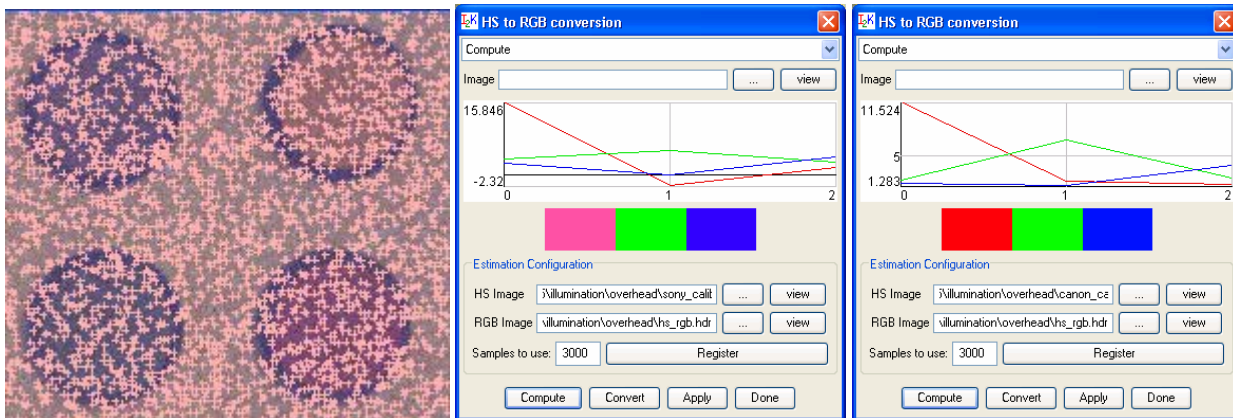


Figure 8: The cloud of crosses (left) denotes the points that were used for establishing the data-driven mapping between two set s of RGB images. The mapping from Sony RGB (middle) and Canon RGB (right) to RGB values derived from HS images.

6 SUMMARY

We presented the utilization of high-spectral resolution imagery for improving low-spectral resolution imagery. We identified two directions for utilization of HS images, such as (a) for evaluation and calibration of RGB colors acquired from commercial color cameras, and (b) for sub-spectral resolution improvement of image quality. Next, we provided an overview of challenges associated with the use of HS information for improving the quality of color imagery due to non-ideal illumination sources and non-ideal hyperspectral camera characteristics, as well as several adjustment (calibration) approaches to compensate for wavelength and spatial dependencies of real acquisition systems.

As one part of this summary, we would like to comment on our experimental results presented in Section 5. One has to be aware that, unfortunately, our hyperspectral camera has several deviations from ideal. For example, one can observe dark speckles in Figure 5 that are part of the calibrated HS image. The dark speckles are due to those cases when measured HS values at a location (x,y) are smaller than the black image values at (x,y) , or larger than the white image values at (x,y) . These values are not only outside of the expected [black pixel, white pixel] range but also temporarily vary which indicates temporal fluctuation of camera acquisition. In the case of an ideal hyperspectral camera, we should not observe these values. In order to perform calibration correctly, we clipped the illumination-calibrated values to min or max reflectance values (0 or 1). The wavelength dependency shown in Figure 3 also cannot be ignored. The small dynamic range for blue wavelengths shown in Figure 3 leads to a significant amount of noise in those hyperspectral bands. We have performed wavelength calibration according to equation (2). However, we have noticed that the blue bands between 400nm-440nm after wavelength-calibration were still achieving smaller dynamic range than other wavelengths. This is attributed to a non-linear model between the exposure time and the number of photons impinging on the CCD sensor for these blue wavelengths. The outcome of this non-linear dependency can be observed in the difference between the blue color obtained from HS images and the blue colors obtained from Sony and Canon cameras (see Figure 7; left upper circle). Therefore, the results presented in Table 2 are viewed as relative comparisons rather than absolute comparisons. We could hypothesize that if the goal would be to predict RGB values of a specific color camera from hyperspectral measurements then a data-driven mapping from high-spectral dimensional space to low-spectral dimensional space might be the best approach to perform the HS to RGB mapping.

Having described all our concerns about the hyperspectral camera used in our work, we believe that the contribution of this paper lies in describing the utilization of HS images for improving RGB color quality of color images as shown in Figure 1. Furthermore, the summary of evaluation and calibration issues provided in Table 1 raises awareness about the calibration difficulties of low-spectral resolution imagery with high-spectral resolution imagery.

ACKNOWLEDGEMENTS

This material is based upon work partially supported by the National Center for Advanced Secure Systems Research (NCASSR), and the National Laboratory for Advanced Data Research (NLADR).

REFERENCES

- 1 Dana, K.J., et al., Reflectance and texture of real-world surfaces. ACM Transactions on Graphics, 1999. 18(1): p. 1-34.
- 2 Dana, K.J. and S.K. Nayar. Correlation Model for 3D Texture. in International Conference Computer Vision. 1999.
- 3 Slipfker, J.F. and S.S. Shapiro, The Johnson System: Selection and Parameter Estimation. Technometric, 1980. 22(2): p. 239-246.
- 4 Sony camera. Available at <http://www.camerasuperstore.com/sonsnnetcolc.html>.
- 5 Official Opto-Knowledge Systems Inc. website. Available at <http://www.techexpo.com/WWW/opto-knowledge/index.html>
- 6 T. Chrien, C. Chovit and P. Miller. "Imaging Spectrometry Using Liquid Crystal Tunable Filters". Jet Propulsion Laboratory and Cambridge Research & Instrumentation Inc.

- 7 Gat, N. ["Imaging Spectroscopy Using Tunable Filters: A Review."](#) Proc. SPIE Vol. 4056, p. 50-64, Wavelet Applications VII, Harold H. Szu, Martin Vetterli; William J. Campbell,, James R. Buss, Ed. (Invited paper). Publ. Date: 04/2000.
- 8 Kooper R., P. Bajcsy and D. Andersh, "Methodology for Evaluating Statistically Predicted Versus Measured Imagery" SPIE 2005, Algorithms for SAR Imagery XII, 28 March - 1 April 2005, Orlando (*Kissimmee*), Florida USA.
- 9 Varma, M. and A. Zisserman. Classifying Images of Materials: Achieving Viewpoint and Illumination Independence. Proceedings of the 7th European Conference on Computer Vision in Copenhagen, Denmark, Vol 3. Springer-Verlag, May 2002, pp 255—271.
- 10 CURet Database; URL: <http://www1.cs.columbia.edu/CAVE/curet/>
- 11 Brodatz P., "Textures: A Photographic Album for Artists and Designers", Dover Publications, New York, 1966.
- 12 VisTex Databases; URL: <http://www-white.media.mit.edu/vismod/imagery/VisionTexture/vistex.html>
- 13 Bajcsy P., R. Kooper and D. Andersh, "Multisensor Scene Modeling Using Statistical Models for Bidirectional Texture Functions," Proceedings of SPIE 2004, Algorithms for SAR Imagery XI, April 12-15, 2004. Vol. 5427, [5427-30].
- 14 Image to Knowledge (I2K), a library of software tools developed at NCSA/UIUC, web documentation at <http://alg.ncsa.uiuc.edu/tools/docs/i2k/manual/index.html>.
- 15 Ramanath R., W. E. Snyder, Y. Yoo and M.S. Drew, "Color Image Processing Pipeline," IEEE Signal Processing Magazine, Vol. 22, No. 1., January 2005, pp 34-43.
- 16 Dan Bruton, "Color Science", <http://www.cox-internet.com/ast305/color.html>
- 17 Oriol Xenon Lamp, European Synchrotron Radiation Facility (ESRF), <http://www.newport.com/store/product.aspx?lone=Light+Sources<wo=Light+Sources&id=5276&lang=1§ion=Specs>
- 18 Benediktsson, J. A., J. R. Sveinsson and K. Arnason, 1995, Classification and feature extraction of AVIRIS data. IEEE Transactions on Geoscience and Remote Sensing 33, 1194-1205.
- 19 Csillag, F, L. Pasztor, and L. Biehl, 1993, Spectral band selection for the characterization of salinity status of soils. Remote Sensing of Environment 43, 231-242.
- 20 Healey, G., and D.A. Slater, 1999. Invariant Recognition in Hyperspectral Images, *IEEE Proceedings of CVPR99*, pp. 438-443.
- 21 Merényi, E., W.H. Farrand, L.E. Stevens, T.S. Melis, and K. Chhibber, 2000. Mapping Colorado River Ecosystem Resources In Glen Canyon: Analysis of Hyperspectral Low-Altitude AVIRIS Imagery, *Proceedings of ERIM, 14th Int'l Conference and Workshops on Applied Geologic Remote Sensing*, November 4-6, Las Vegas, Nevada, pp. 44-51.
- 22 Yamagata, Y., 1996. Unmixing with Subspace Method and Application to Hyper Spectral Image, *Journal of Japanese Society of Photogrammetry and Remote Sensing*, Vol.35, pp. 34-42.
- 23 Bajcsy P., and P. Groves, "Methodology For Hyperspectral Band Selection," *Photogrammetric Engineering and Remote Sensing journal*, Vol. 70, Number 7, July 2004, pp. 793-802